BALNEO RESEARCH Balneo and PRM Research Journal
English Edition
e ISSN 2734 - 8458 p ISSN 2734 - 844X ROMANIAN ASSOCIATION OF BALNEOLOGY

Research article

A hyperspectral index-based approach for in vivo automatic detection of skin tumors from hyperspectral images

Mihaela Antonina Calin [1], Dragos Manea [1], Andrei Dumitrescu [2], Sorin Viorel Parasca [2,3]

1 National Institute of Research and Development for Optoelectronics – INOE 2000, Magurele, Romania
2 Emergency Clinical Hospital for Plastic, Reconstructive Surgery and Burns, Bucharest, Romania
3 Carol Davila University of Medicine and Pharmacy, Bucharest, Romania

* Correspondence: manea.dragos88@gmail.com, manea.dragos@inoe.ro

Citation: Calin M.A., Manea D., Dumitrescu A., Parasca S.V. - A hyperspectral index-based approach for in vivo automatic detection of skin tumors from hyperspectral images
Balneo and PRM Research Journal ***2023****, 14(4): 640*

Academic Editor(s):
Constantin Munteanu

Reviewer Officer:
Viorela Bembea

Production Officer:
Camil Filimon

Received: 12.12.2023
Accepted: 04.12.2023
Published: 20.12.2023

Reviewers:
Mihail Hoteteu
Elena Valentina Ionescu

Publisher's Note: Balneo and PRM Research Journal stays neutral with regard to jurisdictional claims in published maps and institutional affiliations.

Abstract: Skin cancer is the most common human malignancy and early diagnosis is important for successful treatment. Hyperspectral imaging provides both spectral and spatial information which may be useful for tumor diagnosis. In the present study, hyperspectral images of 36 skin tumors (seborrheic keratosis, actinic keratosis, basal cell carcinoma, squamous cell carcinoma) were acquired and analyzed. A skin cancer index was defined taking into account the differences in the angles made by the spectral slopes of the tumors and normal skin and the x axis in the spectral range (580-600) nm (where the differences in spectral signatures proved to be significant). When compared to histopathological diagnosis, the index allowed for differentiation between benign and malignant tumors and even between seborrheic and actinic keratosis or basal cell carcinoma and squamous cell carcinoma. Benign tumors had an index under 0.39999, while basal cell carcinoma ranged between 0.4000-0.59999, and squamous cell carcinoma between 0.6000-06999. In conclusion, the hyperspectral image-based skin tumor index is an objective method of identification and differentiation of skin tumors and may become a useful tool in their early diagnosis

Keywords: skin cancer hyperspectral index, reflectance, slope, seborrheic keratosis, actinic keratosis, basal cell carcinoma, squamous cell carcinoma.

1. Introduction

Skin cancer is the most frequent human malignancy [1]. Basal cell carcinoma, squamous cell carcinoma and malignant melanoma put a tremendous pressure on health systems around the world and are responsible for a high number of surgeries or other invasive treatment modalities and can lead to a significant degree of functional and esthetic impairment as well as deaths [2]. Fortunately, skin cancers are treatable and have reached high survival rates [3]. Therefore, early diagnosis is of utmost importance. Skin is easily accessible for clinical examination and tumor detection and identification has gained a lot in accuracy with widespread use of dermoscopy as an adjunct to visual exam [4]. Both methods are unfortunately dependent on the physician's experience and generate a significant number of misdiagnoses [4]. The histopathological exam remains the most reliable diagnostic tool, but it is invasive and generates important psychological stress due to the time lapse between the biopsy and the final diagnostic decision [5].

This is the reason for a continuing search for non-invasive and objective investigative methods that can identify and differentiate between skin cancer types. Reflectance confocal microscopy was found to provide good results in diagnosis of basal cell carcinoma [6], in monitoring actinic keratoses [7] or monitoring treatment in patients with malignant melanoma [8]. Optical coherence tomography offers deeper images and has proved useful

in diagnosing non-melanoma skin cancer [9]. High frequency ultrasound had some success in detecting basal cell carcinoma [10], as well as terahertz pulsed imaging [11]. Multispectral imaging has been tested for identification of malignant tumors in the last decade. Delpueyo et al [12] investigated 429 skin lesions (benign, melanomas and BCCs) by extracting 15 parameters from multispectral images and feeding them to a learnig machine with high sensitivity (87.2% for melanomas and 100% for BCCs) but a rather low specificity (54.5%). Stamnes et al [13] reported on discrimination between malign and benign pigmented skin lesions using multispectral and multi-angles images. They used an optical transfer diagnosis device which generated 86 diagnostic paramenters from which they derived a final diagnostic indication tool used for clustering and obtained a sensitivity of 97% for a small data set and 99% for a large data set, with specificities of 97% and 93% respectively. In 2018, Ray Barosso et al [14] used an extended infrared domain combined with the visible one to discriminate between nevi and melanoma with a sensitivity of 78.6% and a specificity of 84.6%.

In the last two decades, hyperspectral imaging has also been successfully tested for several medical applications, including skin tumor detection and differentiation [15]. Recently, Courtenay et al [16] published a study on non-melanoma skin cancer in which hyperspectral imaging and a complex statistical analysis of data were used to differentiate between malignant and benign skin tumors concluding that the optimal wavelength range for tumor detection was (573.45-779.88) nm, while for distinguishing between tumor types was (429.16-520.17) nm. Leon et al [17] studied 76 pigmented tumors using hyperspectral imaging and a framework for automatic detection of the tumor type (malignant or benign) and obtained a sensitivity of 87.5% and a specificity of 100%. Lindholm et al [18] reported good results on 42 skin lesions with hyperspectral imaging with illumination from 3 different angles and a convolutional network (41 tumors were correctly diagnosed). Paoli et al [19] tested a double trained deep neural network and two approaches (pixel-wise classification and majority vote classification) to diagnose malignant melanoma from 325 hyperspectral images of pigmented skin tumors and obtained encouraging results.

This paper proposes a new approach for in vivo automatic detection of skin tumors based on hyperspectral imaging and a skin cancer index defined as a quantitative measure of differentiation among skin tumor types. The proposed skin spectral index, which takes into account the spectral characteristics of both healthy skin and tumors derived from hyperspectral data, offers a new, non-invasive, easy, fast, personalized and low-cost method of differentiating skin tumors that can facilitate the decision-making process regarding the treatment.

In order to fulfill this goal, several steps were undertaken: (1) acquiring hyperspectral images of different skin tumors before excision biopsy; (2) developing a hyperspectral tumor index based on differences among spectra of benign and malign lesions; (3) identification and classification of skin tumors according to spectral index values; (4) comparing the capacity of the proposed approach with the results of histopathological tests; (5) establishing future research directions for expanding the applicability of the method to differentiate between the different forms of basal cell carcinoma or squamous cell carcinoma, melanoma, pigmented lesions.

2. Patients and methods

2.1. Patients

Patients with benign and malignant skin tumors who were admitted to the Emergency Clinical Hospital for Plastic, Reconstructive and Burn Surgery, Bucharest between January and February 2023 were recruited for this study. A total of 36 patients (17 males and 19 females) were included in this study. The average age of the patients was 60.2 years (between 50-83 years). All patients were Caucasians, with Fitzpatrick's skin phenotype ranging from 2 to 4. All skin tumors were excised after hyperspectral images of the tumor and surrounding skin were obtained. The acquisition of the hyperspectral images lasted

between 10 to 20 seconds in all cases, during which the patients were not allowed to move (in case of sudden moves, the procedure was repeated). The specimens were transported in formalin to the pathology lab where standard processing took place. The histopathological diagnosis was received in 7 to 10 days. During that period the hyperspectral images had already been analyzed. Approval for experimental procedures involving human participants was obtained from the ethics committee of the Emergency Clinical Hospital for Plastic, Reconstructive and Burn Surgery and was performed in accordance with the 1964 Helsinki declaration and its subsequent amendments or comparable ethical standards. Informed consent was obtained from all participants prior to enrollment in this study. Among the 36 investigated tumors, 13 were benign and 23 malignant tumors. Benign tumors were actinic keratosis and seborrheic keratosis, while malignant tumor types were basal cell carcinoma and squamous cell carcinoma. (Table 1). All tumors were located in the head area (27 on the face, and 9 on the scalp).

Table 1 The types of investigated tumors

Skin tumor types	Skin tumor sub-types	Number of cases		Total
		Sex		
		F	M	
Benign tumors	actinic keratosis	2	4	**13**
	seborrheic keratosis	4	3	
Malignant tumor	basal cell carcinoma	7	6	**23**
	squamous cell carcinoma	6	4	
Total				**36**

2.2. Hyperspectral image acquisition and processing

Hyperspectral images of tumor areas and adjacent normal skin were acquired using a pushbroom hyperspectral imaging system consisting of an imaging spectrograph (ImSpector V8E, Specim, Oulu, Finland) covering the spectral range (400–800) nm coupled with a charge-coupled device (DX4 camera, Kappa, Gleichen, Germany). This system allows the acquisition of 205 spectral bands at a spectral resolution of 1.97 nm and a frame rate of 41 fps. The hyperspectral system was mounted on a tripod (Manfrotto 055XDB, Cassola, Italy) equipped with a mobile head (Manfrotto MVH502AH). Scanning of the investigated tumor area was performed with a single-axis galvanometer scanning mirror system (GVS211, Thorlabs, New Jersey, USA) equipped with a broadband dielectric mirror (average reflectance > 95% in the spectral range (400 – 750) nm). For uniform illumination of the investigated area an illumination system consisting of two 300 W halogen lamps (OSRAM, Munich, Germany) with diffusion filters (Kaiser Fototechnik GmbH and Co. KG, Buchen, Germany) mounted on a RS1 camera stand (Kaiser Fototechnik GmbH & Co.KG, Buchen, Germany) was used. Hyperspectral images containing both spectral and spatial information about the investigated area were acquired and stored in a computer using SpectralDAQ software (Specim, Oulu, Finland). Processing and subsequent analysis of hyperspectral images was performed using ENVI v.5.1 software (Exelis Visual Information Solutions, Boulder, Colorado, USA).

The acquired hyperspectral images are usually affected by the spatial non-uniformity of artificial light intensity and the dark current effect of the camera sensor [20]. Therefore, in order to solve these problems, an image processing step is necessary to obtain accurate and consistent information. A common calibration technique was applied to all acquired images. This technique is based on the acquisition of black and white reference images and

the derivation of corrected images using Eq. 1.

$$I_c(x,y) = \frac{I_O(x,y) - D(x,y)}{W(x,y) - D(x,y)} \quad (1)$$

where: $I_C(x,y)$ is the calibrated hyperspectral image expressed as reflectance in the spatial position (x,y), $I_O(x,y)$ is the original hyperspectral image in the spatial position (x,y), D(x,y) is the dark reference image at the spatial position (x,y) acquired under the condition of covering the lens of the hyperspectral system with a black cap, and W(x,y) is the white reference image obtained from a 98% polytetrafluoroethylene (PTFE) reference tile (model WS-2, Avantes, Apeldoorn, Netherlands), placed in the investigated scene near the tumor area (Figure 1).

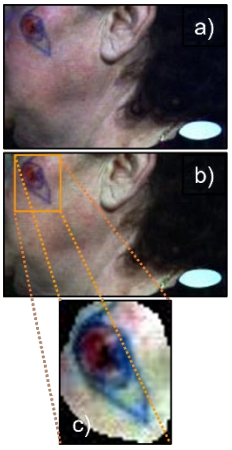

Figure 1. Hyperspectral images of a 55 years old female patient with a squamous cell carcinoma of the cheek: a) original hyperspectral image (I_O); b) calibrated reflectance image (I_C); c) region of interest image (ROI) related only to the tumor area and adjacent normal skin

As can be seen in Figure 1b, the calibrated reflectance image (I_C) contains a large amount of redundant information that can influence the subsequent image analysis and increase the computation time. Therefore, the selection of a region of interest (ROI image) containing only the tumor area and the adjacent normal skin was a necessary processing step for the calibrated images. The selection was done manually from hyperspectral images acquired from each patient by the plastic surgeon who performed the excision, and the size of the region of interest was roughly matched to that of the tumor plus a band of normal skin (Figure 1c). These ROIs were used as the bases for further spectral analysis of skin tumor images.

2.3. Spectral characteristics analysis and detection of skin tumor type

The spectral characteristics of different malignant and benign skin tumors extracted from hyperspectral data were analysed in terms of wavelength, intensity, and shape. Spectral differences between malignant and benign tissues were measured with a new skin index, namely the hyperspectral imaging-based skin cancer index (HSI-SCI) focused on the slope and curvature of the reflectance spectra of tissue types. Reflectance spectra extracted from 15 pixels in the normal and tumor area of each ROI image were averaged to generate a single mean reflectance spectrum for each region in the ROI (Figure 2). The 15 pixels were manually selected by a physician (plastic surgeon) from inside the macroscopic margins of the tumor, or at several milimeters to up 1 cm from the tumoral margin for normal skin (when the tumor had and excision marking drawn by the surgeon, the normal skin pixels were selected from outside the marking, and the marking itself was avoided).

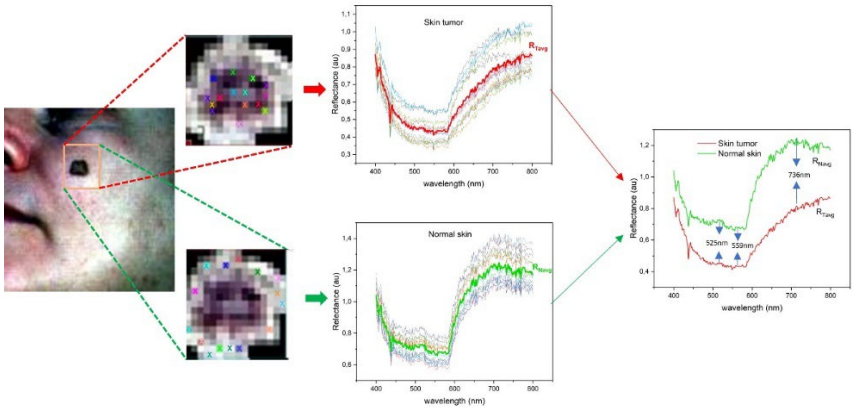

Figure 2. Spectral profiles of tumoral and normal skin in different pixels in the ROI (normal and tumoral area) and their average spectral profiles

It is noteworthy in Figure 2 that the average spectral profiles of tumor and normal skin are different both in shape and intensity values. The only common element is the inflection point in the red spectral range. This aspect was used in the development of the hyperspectral imaging-based skin cancer index (HSI-SCI) that allows the differentiation between benign and malignant tissue.

In defining the HSI-SCI index, the differences between the rates of change of the average reflectance spectra of tumoral and normal tissues ($\Delta R/\Delta\lambda$) over a particular spectral range centered on the inflection point were evaluated (Figure 3).

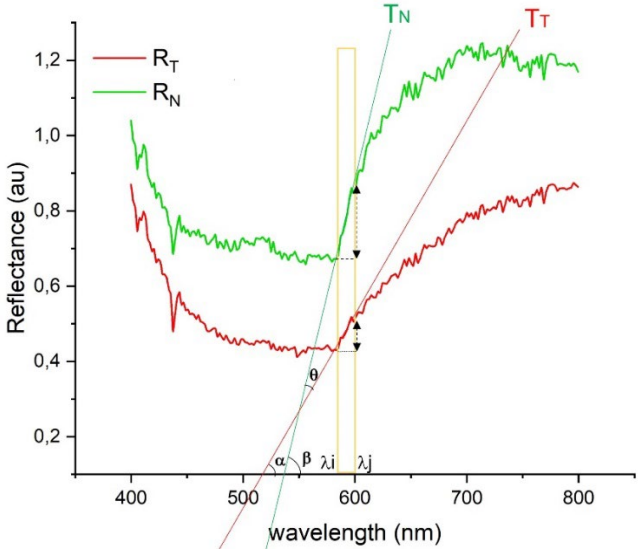

Figure 3. The average reflectance spectra of tumoral and normal tissues and the spectral parametres included in the definition of the HSI-SCI index

The reflectance change rate for the two types of tissues, normal and tumoral, was expressed by the following equations:

$$\frac{\Delta R_N(\lambda)}{\Delta\lambda} = \frac{R_N(\lambda_j) - R_N(\lambda_i)}{\lambda_j - \lambda_i} = \tan\beta \quad (2)$$

$$\frac{\Delta R_T(\lambda)}{\Delta\lambda} = \frac{R_T(\lambda_j) - R_T(\lambda_i)}{\lambda_j - \lambda_i} = \tan\alpha \quad (3)$$

where: $R_N(\lambda)$ and $R_T(\lambda)$ are the reflectance values of normal and tumor tissue at wavelengths λ_i and λ_j. The rates of reflectance change can be correlated with the angles between the tangent lines to the reflectance spectra of tumor ($R_T(\lambda)$) and normal ($R_N(\lambda)$)

tissues at data points in the spectral range (λ_i, λ_j), respectively with the angles α and β formed by the tangents T_N and T_T with the x axis which also defines the slopes of these tangent lines according to the following expressions:

$$S_T = \tan\alpha \quad (4)$$
$$S_N = \tan\beta \quad (5)$$

where: S_T and S_N represent the slopes of the tangent lines T_T and T_N to the reflectance spectra of tumoral and normal tissues, respectively.

The differences between these slopes were evaluated by calculating the angle (θ) between the two tangents according to the following expression:

$$\theta = \beta - \alpha \quad (6)$$

By applying the tangent function to Equation 6 results the following expression:

$$\tan\theta = \tan(\beta - \alpha) = \frac{\tan\beta - \tan\alpha}{1+\tan\beta\tan\alpha} \quad (7)$$

The HSI-SCI index was defined as difference between the slopes by the following expression:

$$\%\text{HSI} - \text{SCI} = 100 \text{ x } \tan\theta \quad (8)$$

By inserting Equation 4 and Equation 5 into Equation 8 results in the definition expression of the HSI-SCI index as follows:

$$\%\text{HSI} - \text{SCI} = \left|\frac{S_T - S_N}{1+S_T S_N}\right| \text{x } 100 \quad (9)$$

In summary, based on Equation 9, a new in vivo skin tumor detection modality based on skin spectral index is proposed alongside histopathological and clinical examinations. The higher values of the HSI-SCI index correspond to a large difference between the slopes ($\theta > 30^0$) associated with malignant tumors and the lower values correspond to small differences between the slopes characteristic of benign tumors, thus making possible a clear differentiation of the tumor types. Moreover, this HSI-SCI index allows the differentiation between the different types of benign tumors (actinic keratosis, seborrheic keratosis etc.) or malignant (BCC, SCC) not only between the broad benign/malignant categories.

2.4. Statistical analysis

Data analysis was performed based on Pearson correlation coefficients calculated to assess how strong the relationship is between the HSI-SCI index and tumor type. All statistical calculations in this study were performed using SPSS software v23 (International Business Machines Corporation (IBM), New York, United States).

3. Results

3.1. Spectral characteristics of different skin tumors types

Representative reflectance spectra extracted from ROI images of different types of benign and malignant skin tumors as well as normal skin are shown in Figure 4.

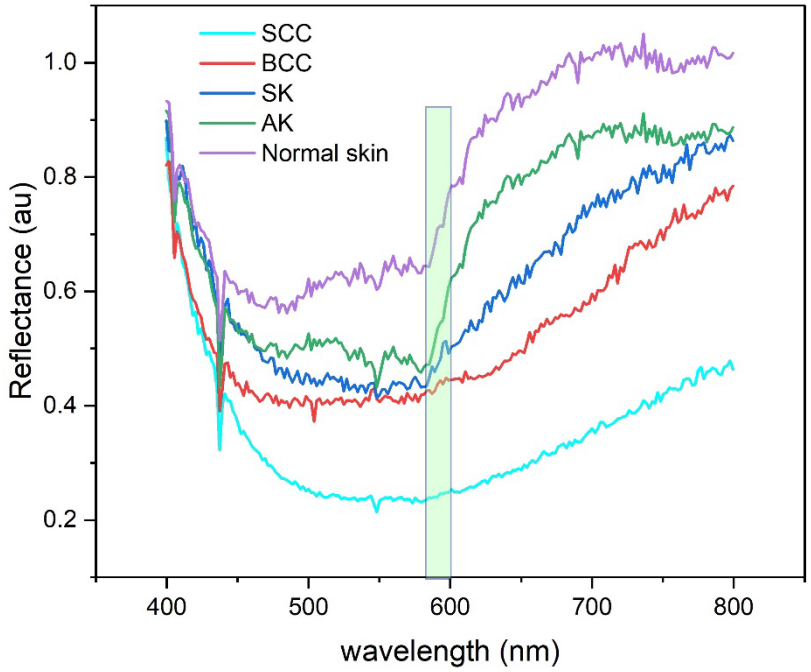

Figure 4. Reflectance spectra of different types of benign and malignant skin tumors and normal skin in the visible spectral range (400-800) nm

As depicted in Figure 4, the trends in the reflectance spectra of AK tumors are basically the same as those of normal skin. Three main peaks can be noted in both reflectance spectra located around the wavelengths of 525 nm, 559 nm, and 736 nm, the difference being the reflectance values corresponding to each peak which for the AK tumor are lower than those of normal skin.

In the SK, important changes in the reflectance spectrum are highlighted by the minimization of the first two peaks and an increase in the reflectance values in the spectral range (583-800) nm. Malignant tumors (BCC and SCC) show a similar shape of the reflectance spectra with an important decrease in reflectance values in the first part of the spectrum (400-550) nm and a less steep increase in the final part of the spectrum (starting from 583 nm), without any relevant peak.

Taking into account these important differences in the spectral characteristics of benign and malignant lesions, the only common element for comparing and differentiating them was identified as the wavelength from which the reflectance values start to increase in all cases, called the inflection point. From the analysis of the spectral data it emerged that this inflection point was located at $\lambda = 583$ nm for all types of tumoral and normal tissues. Therefore, among the 205 spectral bands contained in the ROI images covering the entire spectral range from 400 to 800 nm, only a narrow spectral range from $\lambda_i = 583$ to $\lambda_j = 600$ nm, containing 15 spectral bands, was selected for subsequent calculation of reflectance change rate for all tissues types and the differentiation of benign and malignant tumors based on the HSI-SCI index.

3.2. Detection of different skin tumors type using HSI-SCI index

The values of the HSI-SCI index calculated for different skin tumors types fall into four clusters, allowing a clear differentiation of benign tumors from malignant ones as well as the different subtypes included in the two main categories (Figure 5).

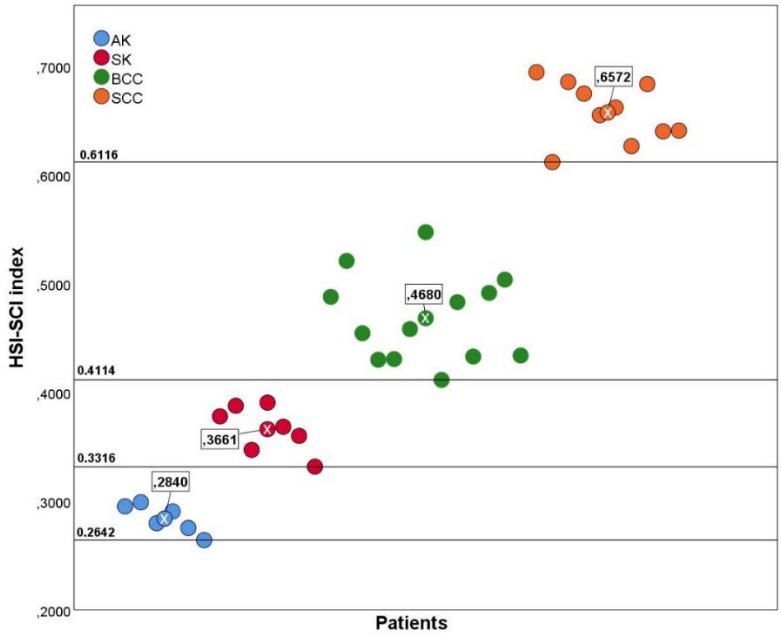

Figure 5. Scatter plot between HSI-SCI index of each patient and skin tumor type for all participants in the study

As can be seen in Figure 5, the data points are clearly grouped into four clusters (blue, red, green, and orange) corresponding to the four types of skin tumors investigated in this study (actinic keratosis (AK), seborrheic keratosis (SK), basal cell carcinoma (BCC) and squamous cell carcinoma (SCC)). No overlap of the clusters is observed. The blue cluster is of AK which tends to have the lowest HSI-SCI index values, centered around the median value of 0.2840. The highest HSI-SCI index values are grouped in the orange cluster representing SCC tumors. A median HSI-SCI index value of 0.6572 represents the center of this cluster. The data points belonging to the red group associated with SK tumors have a median HSI-SCI index value (0.3661) higher than that of AK, but lower than the one of the BCC cluster. An intermediate median value of the HSI-SCI index was found for the BCC data points (0.4680). AK and SK clusters show a strong and moderate, negative, linear correlation between HSI-SCI index and tumor type (r_{AK} = - 0.868, r_{SK}= - 0.619). The BCC clusters, however, show a very weak negative, linear correlation (r_{BCC} = - 0.101) while the SCC show a weak negative, linear correlation (r_{SCC} = - 0.289). Taking into account the negative correlation of all clusters and the reference lines corresponding to their minimum values (shown in Figure 5), the ranges of HSI-SCI index values for each type of benign or malignant skin tumor were identified and are shown in Table 2.

Table 2. HSI-SCI index for the benign and malign skin types

Skin tumor type	Skin tumor subtype	HSI-SCI index
Benign tumors	actinic keratosis	< 0.2999
	seborrheic keratosis	0.3000- 0.3999
Malignant tumor	basal cell carcinoma	0.4000-0.5999
	squamous cell carcinoma	0.6000-0.6999

The calculated HSI-SCI index values show that a precise quantitative differentiation among different types of skin cancers is possible in addition to the qualitative differentiation provided by spectral fingerprints.

3. Discussion

The present study investigated the ability of hyperspectral imaging to differentiate among several types of benign and malignant skin tumors. The analysis of the spectra of normal and diseased skin has shown that in the spectral range (583-600) nm, reflectance values displayed a raise. This raise was higher for normal skin, and it became lower for benign tumors and even lower for BCC and SCC. The angles made by the tangent lines to the reflectance spectra with the x axis in this zone of the spectra seemed to be a good criterion for differentiating normal tissue, benign, and malignant tumors. In order to compensate for individual characteristics, the difference between the angle of the patient's normal skin spectrum and the angle of the tumor's spectrum was used as a base for the above defined hyperspectral imaging-based skin cancer index. The results were very encouraging, showing a clear distinction between benign and malignant and even among different types of tumors in each category. The correlation between histopathological diagnosis and the values of the index was very good. Thus, an objective quantitative criterion for tumor differentiation in hyperspectral images was developed for the first time, to our knowledge. This could be a great help for the surgeon treating un-biopsied skin tumors in order to give some orientation about the needed extent of the excision even before definitive pathological diagnosis. It could also prove to be a reliable screening method, alongside clinical examination.

Several other researchers have investigated the value of hyperspectral imaging in skin tumor detection and characterization. Courtenay et al [16] used hyperspectral imaging and complex statistical data analysis for characterization of non-melanoma skin cancer. The spectral range they found significant for tumor detection was (573.45-779.88) nm, a range which includes our much narrow interval. For tumor differentiation, the significant spectral range was reported as (429.16-520.17) nm, a zone where even our study found important differences in reflectance values. Yet, the method described in the present study is simpler and more reliable, at least for the investigated group. Salmivuori et al [21] used hyperspectral imaging to detect tumor margins in 16 BCCs of the head and neck with good results. They also used artificial intelligence for spectral data processing. Räsänen and colleagues [22] reported good results with hyperspectral imaging and machine learning in differentiating melanoma from pigmented BCCs. Again, data analysis was more complex compared to the present study.

Therefore, the advantages of our method are its computational simplicity (without the need for machine learning) and its reliability (there was no overlap of calculated indices between adjacent categories). This study has its limitations. The most important one is the relatively small number of investigated tumors, which lowers the power of our results. Another consequence was that only two types of benign lesions (seborrheic keratosis and actinic keratosis) and only non-melanoma skin cancer were included in the study. The extent of the group did not permit detailing within each cancer group (subtypes of BCC or SCC). The absence of malignant melanoma may be another limitation, as it represents a serious threat and it is a subject of continuous investigation [18, 19].

The study produced new directions of research. A larger, prospective study would be needed for validation of the method, grouping the tumors according to their indices and then comparing the results with the pathology exam. An extension of the hyperspectral-based index in the study of pigmented lesions, especially malignant melanoma, could provide interesting results.

4. Conclusions

In conclusion, hyperspectral imaging is useful in characterization of skin tumors, with its derived skin cancer index being an objective, quantitative, reliable tool for differentiating among tumors (benign from malign or even inside each group).

Acknowledgments: This work was funded by the Romanian Ministry of Research, Innovation and Digitization through the Core Program within the National Research Development and Innovation Plan 2022-2027 grant PN23 05 (11N/03.01.2023) and Program No.1 - Development of the National Research and Development System, Subprogram 1.2 - Institutional Performance - Projects for financing excellence in R&D grant no. 18PFE/30.12.2021.

Author Contributions: All the authors have equal contribution

Funding: This research received no external funding

Institutional Review Board Statement: Not applicable.

Informed Consent Statement: Not applicable.

Data Availability Statement: Not applicable

Conflicts of Interest: The authors declare no conflict of interest

.

References

1. Linares MA, Zakaria A, Nizran P. Skin Cancer. Prim Care. 2015 Dec;42(4):645-59. doi: 10.1016/j.pop.2015.07.006. PMID: 26612377.
2. Gordon R. Skin cancer: an overview of epidemiology and risk factors. Semin Oncol Nurs. 2013 Aug;29(3):160-9. doi: 10.1016/j.soncn.2013.06.002. PMID: 23958214.
3. Heibel, H.D.; Hooey, L.; Cockerell, C.J. A Review of Noninvasive Techniques for Skin Cancer Detection in Dermatology. Am. J. Clin. Dermatol. 2020, 21, 513–524.
4. Yilmaz, A.; Gencoglan, G.; Varol, R.; Demircali, A.A.; Keshavarz, M.; Uvet, H. MobileSkin: Classification of Skin Lesion Images Acquired Using Mobile Phone-Attached Hand-Held Dermoscopes. J. Clin. Med. 2022, 11, 5102.
5. Pathania, Y.; Apalla, Z.; Salerni, G.; Patil, A.; Grabbe, S.; Goldust, M. Non-Invasive Diagnostic Techniques in Pigmentary Skin Disorders and Skin Cancer. J. Cosmet. Dermatol. 2022, 21, 444–450.
6. Lupu, M.; Popa, I.M.; Voiculescu, V.M.; Caruntu, A.; Caruntu, C. A Systematic Review and Meta-Analysis of the Accuracy of in vivo Reflectance Confocal Microscopy for the Diagnosis of Primary Basal Cell Carcinoma. J. Clin. Med. 2019, 8, 1462.
7. Kim, Y.-S.; Shin, S.; Jung, S.-H.; Park, Y.M.; Park, G.S.; Lee, S.H.; Chung, Y.-J. Genomic Progression of Precancerous Actinic Keratosis to Squamous Cell Carcinoma. J. Investig. Dermatol. 2022, 142, 528–538.e8.
8. Hibler, B.P.; Yélamos, O.; Cordova, M.; Sierra, H.; Rajadhyaksha, M.; Nehal, K.S.; Rossi, A.M. Handheld reflectance confocal microscopy to aid in the management of complex facial lentigo maligna. Cutis 2017, 99, 346–352.
9. Themstrup, L.; Jemec, G.B.E. Chapter 6—Optical Coherence Tomography for Skin Cancer and Actinic Keratosis; Hamblin, M.R., Avci, P., Gupta, G.K.B.T.-I.D., Eds.; Academic Press: Boston, MA, USA, 2016; pp. 59–67. ISBN 978-0-12-802838-4.
10. De Barcaui, E.O.; Carvalho, A.C.P.; Valiante, P.M.; Piñeiro-Maceira, J.; Barcaui, C.B. High-frequency (22-MHz) ultrasound for assessing the depth of basal cell carcinoma invasion. Ski. Res. Technol. 2021, 27, 676–681.
11. Woodward, R.M.; Cole, B.E.; Wallace, V.P.; Pye, R.J.; Arnone, D.D.; Linfield, E.H.; Pepper, M. Terahertz pulse imaging in reflection geometry of human skin cancer and skin tissue. Phys. Med. Biol. 2002, 47, 3853–3863.
12. Delpueyo, X.; Vilaseca, M.; Royo, S.; Ares, M.; Rey-Barroso, L.; Sanabria, F.; Puig, S.; Malvehy, J.; Pellacani, G.; Noguero, F.; Solomita, G.; Bosch, T. Multispectral imaging system based on light-emitting diodes for the detection of melanomas and basal cell carcinomas: a pilot study. J. Biomed. Opt. 22(6) 065006 (29 June 2017) https://doi.org/10.1117/1.JBO.22.6.065006
13. Stamnes, J.; Ryzhikov, G.; Biryulina, M.; Hamre, B.; Zhao, L.; Stamnes, K. Optical detection and monitoring of pigmented skin lesions. Biomed. Opt. Express 8, 2946-2964 (2017).

14. Rey-Barroso, L.; Burgos-Fernández, F. J.; Delpueyo, X.; Ares, M.;Royo, S.; Josep Malvehy, J.; Puig, S.; Vilaseca, M. Visible and extended infra-red multispectral imaging for skin cancer diagnosis. Sensors.2018;18:1441. doi:10.3390/s18051441.
15. Karim S, Qadir A, Farooq U, Shakir M, Laghari AA. Hyperspectral Imaging: A Review and Trends towards Medical Imaging. Curr Med Imaging. 2022 May 19. doi: 10.2174/1573405618666220519144358. Epub ahead of print. PMID: 35598236.
16. Courtenay LA, González-Aguilera D, Lagüela S, Del Pozo S, Ruiz-Mendez C, Barbero-García I, Román-Curto C, Cañueto J, Santos-Durán C, Cardeñoso-Álvarez ME, Roncero-Riesco M, Hernandez-Lopez D, Guerrero-Sevilla D, Rodríguez-Gonzalvez P. Hyperspectral imaging and robust statistics in non-melanoma skin cancer analysis. Biomed Opt Express. 2021 Jul 20;12(8):5107-5127. doi: 10.1364/BOE.428143. PMID: 34513245; PMCID: PMC8407807.
17. Leon R, Martinez-Vega B, Fabelo H, Ortega S, Melian V, Castaño I, Carretero G, Almeida P, Garcia A, Quevedo E, Hernandez JA, Clavo B, M Callico G. Non-Invasive Skin Cancer Diagnosis Using Hyperspectral Imaging for In-Situ Clinical Support. J Clin Med. 2020 Jun 1;9(6):1662. doi: 10.3390/jcm9061662. PMID: 32492848; PMCID: PMC7356572.
18. Lindholm V, Raita-Hakola AM, Annala L, Salmivuori M, Jeskanen L, Saari H, Koskenmies S, Pitkänen S, Pölönen I, Isoherranen K, Ranki A. Differentiating Malignant from Benign Pigmented or Non-Pigmented Skin Tumours-A Pilot Study on 3D Hyperspectral Imaging of Complex Skin Surfaces and Convolutional Neural Networks. J Clin Med. 2022 Mar 30;11(7):1914. doi: 10.3390/jcm11071914. PMID: 35407522; PMCID: PMC8999463.
19. Paoli J, Pölönen I, Salmivuori M, Räsänen J, Zaar O, Polesie S, Koskenmies S, Pitkänen S, Övermark M, Isoherranen K, Juteau S, Ranki A, Grönroos M, Neittaanmäki N. Hyperspectral Imaging for Non-invasive Diagnostics of Melanocytic Lesions. Acta Derm Venereol. 2022 Nov 14;102:adv00815. doi: 10.2340/actadv.v102.2045. PMID: 36281811; PMCID: PMC9811300.
20. Polder G, Gerie WAM, Van DH. Calibration and characterization of imaging spectrographs. *Near Infrared Spectroscopy* 2003;11:193-210,.
21. Salmivuori M, Neittaanmäki N, Pölönen I, Jeskanen L, Snellman E, Grönroos M. Hyperspectral imaging system in the delineation of Ill-defined basal cell carcinomas: a pilot study. J Eur Acad Dermatol Venereol. 2019 Jan;33(1):71-78. doi: 10.1111/jdv.15102. Epub 2018 Jun 20. PMID: 29846972.
22. Räsänen J, Salmivuori M, Pölönen I, Grönroos M, Neittaanmäki N. Hyperspectral Imaging Reveals Spectral Differences and Can Distinguish Malignant Melanoma from Pigmented Basal Cell Carcinomas: A Pilot Study. Acta Derm Venereol. 2021 Feb 19;101(2):adv00405. doi: 10.2340/00015555-3755. PMID: 33521835; PMCID: PMC9366698.